



ELSEVIER

Available online at www.sciencedirect.com

SCIENCE @ DIRECT®

Earth and Planetary Science Letters 233 (2005) 325–336

EPSL

www.elsevier.com/locate/epsl

Nanocrystalline (Mg, Fe, Cr)TiO₃ perovskite inclusions in olivine from a mantle xenolith, Udachnaya-East kimberlite pipe, Siberia

Richard Wirth^{a,*}, Stanislav Matsyuk^b

^aGeoForschungsZentrum Potsdam, Div.4, Telegrafenberg, D-14473 Potsdam

^bInstitute of Geochemistry, Mineralogy and Ore Formation, National Academy of Sciences of Ukraine, Palladin Ave., 34,03680 Kyiv-142, Ukraine

Received 19 July 2004; received in revised form 10 January 2005; accepted 18 January 2005

Available online 18 April 2005

Editor: E. Bard

Abstract

Olivine grains from an ilmenite–garnet–peridotite nodule from the kimberlite pipe Udachnaya–Wostotschnaya, Siberia have been investigated by TEM methods (electron diffraction, HREM, AEM, EELS). The nodule is a high-temperature garnet peridotite, which equilibrated at about 1200–1300 °C and 200 km depth. TEM investigation of several olivine grains revealed nanometre-sized inclusions of (Mg,Fe,Cr)TiO₃ perovskite together with ilmenite. Both types of inclusions exhibit a typical grain size of about 50 nm. The crystal structure of the perovskite inclusions is monoclinic with $a_0=1.095$ nm, $b_0=0.5169$ nm, $c_0=0.743$ nm and the monoclinic angle $\beta=95^\circ$. The orientation relationship between perovskite and olivine is $(101)_{ol} // (300)_{per}$ and $[010]_{ol} // [0\bar{1}0]_{per}$. This observation combined with the experimentally determined ilmenite/perovskite phase boundary [A. Metha, K. Leinenweber, A. Navrotsky, M. Akaogi, Calorimetric study of high-pressure polymorphism in FeTiO₃: stability of the perovskite phase, *Phys. Chem. Minerals*, 21 (1994) 207–212] [8] allows the use of perovskite in olivine as a geobarometer. The presence of perovskite in olivine suggests that the peridotite originated at pressures of 8–10 GPa, significantly higher than the pressure of last silicate equilibration (4.5–6.5 GPa).

© 2005 Elsevier B.V. All rights reserved.

Keywords: ilmenite; perovskite; xenoliths; kimberlite; TEM

1. Introduction

Rod-shaped precipitates of (Mg,Fe)TiO₃ in olivine have recently excited the attention of earth scientists.

Based primarily on evidence of abundant exsolution lamellae of (Mg,Fe)TiO₃ ilmenite in olivine a possible exhumation of a garnet lherzolite of Alpe Arami from greater than 300 km depth in the Earth's mantle was derived [1,2]. The authors inferred that ilmenite rods in Alpe Arami olivine exsolved as FeTiO₃ perovskite during the polymorphic transformation of wadsleyite. The conclusions from that observation are still debated [3].

* Corresponding author. Tel.: +49 331 288 1371; fax: +49 331 288 1402.

E-mail address: wirth@gfz-potsdam.de (R. Wirth).

Experimental data on the stability of FeTiO_3 polymorphs are now available over a wide pressure and temperature range. Ilmenite is the stable phase of FeTiO_3 at ambient pressure. The trigonal crystal structure of ilmenite (FeTiO_3) with space group $R\bar{3}$ was confirmed at high pressure and room temperature (up to 3.46 GPa), and at high temperature and ambient pressure (up to 1050 °C) [4]. A phase transition of FeTiO_3 was observed at very high pressure and high temperature. That material, quenched from 20 GPa and 1273 K, had a lithium niobate structure with hexagonal unit cell like ilmenite but with space group $R3c$ [5,6]. Several years later, an additional phase transformation was observed, which showed that the lithium niobate structure of ilmenite transforms reversibly at 16 GPa and room temperature to a perovskite-like phase with an orthorhombic cell [7]. Upon decompression of that phase, perovskite transforms back to the lithium niobate structure, which can be recovered. Calorimetric study of the high-pressure polymorphs of FeTiO_3 proved that the stable form of FeTiO_3 at high pressure and temperature is the perovskite and not the lithium niobate structure [8]. Consequently, the phase transformation observed in quenched material from 20 GPa [5] is a result of the back transformation of the perovskite structure to the lithium niobate structure, which was quenchable. Finally, exceeding 22 GPa, ilmenite with perovskite structure breaks down to “FeO” and TiO_2 [9]. Structural data of the different ilmenite polymorphs are presented in Table 1. Experiments using the Fe–Mg solid solution in lithium niobate and perovskite

structures at high pressures and temperatures show that the pressure for the transition of ilmenite to perovskite (or lithium niobate) structure increases with Mg content [10]. The high-pressure phase transformation of ilmenite to perovskite was suggested as a possible geobarometer provided the transformation would be preserved during kimberlite ascent [8].

In the present paper, we report the first observation of naturally occurring $(\text{Mg,Fe,Cr})\text{TiO}_3$ perovskite as nanometre-sized inclusions preserved in olivine from the kimberlite pipe Udachnaya, Siberia. In P – T space the presence of $(\text{Mg,Fe,Cr})\text{TiO}_3$ perovskite implies a minimum pressure of about 8–10 GPa for the investigated xenolith host, based on the shield geotherm [11] together with the phase boundaries ilmenite/perovskite [8] and olivine/ β -olivine [12]. This finding sheds new light on the composition of the Earth’s mantle beneath the Siberian platform.

2. Sample description

The investigated olivine grains were separated from a porphyroclastic ilmenite–garnet peridotite nodule from the kimberlite pipe Udachnaya–Wostotschnaya, Siberia. The xenolith consists of dark-red-orange garnet (average grain size 2–3 mm), light brown olivine (average grain size 1–2 mm), yellow green clinopyroxene (1–2 mm) and accessory ilmenite with a composition of $(\text{Mg}_{0.404} \text{Fe}_{0.686} \text{Cr}_{0.013})_{1.093} \text{Ti}_{0.925} \text{O}_3$. Accessory ilmenite is present as grains in the xenolith matrix and as syngenetic inclusions (0.1–0.25 mm) in garnet (Table 2). Orthopyroxene is absent. Occasionally, intergrowth of ilmenite and garnet was observed. The groundmass of the xenolith, mainly consisting of olivine is extensively serpentinized. The olivine grains investigated in this study are the unaffected relicts of larger serpentinized crystals. This type of xenolith has been formed in the graphite–pyrope facies [13]. The porphyroclastic ilmenite–garnet peridotites are suggested to have crystallized in a pressure range of 35–40 kbar at temperatures in the range of 1300–1400 °C [14]. However, based on data from a recent paper on Udachnaya peridotite xenoliths, the investigated nodule would belong to the high-temperature garnet

Table 1
Structural data of ilmenite (Mg, Fe) TiO_3 polymorphs

FeTiO ₃	Ilmenite ^a trigonal (space group $R\bar{3}$)	Li–NbO ₃ - structure ^b trigonal (space group $R3c$)	Perovskite ^c orthorhombic	Perovskite (this work) monoclinic
a_o (nm)	0.5088	0.51233	0.5022	1.09(5)
b_o (nm)			0.5169	0.5169 ^d
c_o (nm)	1.4088	1.37602	0.7239	0.74(2)
β				95°

^a Wechsler and Prewitt (1984) [4].

^b Leinenweber (1995) [6].

^c Leinenweber (1991) [7].

^d From Leinenweber (1991) [7].

Table 2

Microprobe analyses from olivine, garnet, cpx and accessory ilmenite grains from the host xenolith (ilm–garnet peridotite) and AEM analyses from ilmenite polymorph inclusions in olivine

Oxide	Wt.% Olivine (EMP)	Wt.% Ilmenite (grain 1; EMP)	Wt.% Ilmenite (grain 2; EMP)	Wt.% Ilmenite in olivine (AEM)	Wt.% Perovskite in olivine (AEM)	Wt.% Garnet (AEM)	Wt.% CPX (AEM)
SiO ₂	40.00	0.05	0.04			41.14	54.26
TiO ₂	0.06	52.72	50.55	49.32	49.67	0.76	0.29
Al ₂ O ₃	0.01	0.76	0.75			20.69	2.19
Cr ₂ O ₃	0.00	1.10	0.70	3.45	6.69	1.13	0.3
FeO	13.49	34.12	33.69	37.75	40.09	11.25	4.51
Fe ₂ O ₃						1.02	1.46
MnO	0.13	0.30	0.26			0.38	0.12
MgO	45.52	10.26	11.13	9.48	3.52	18.27	16.96
CaO	0.05	0.06	0.00			4.54	17.72
Na ₂ O						0.1	1.68
K ₂ O							0.1
Σ	99.26	99.37	97.12	100.00	99.97	99.28	99.59

(Means of 8 analyses each from the two different ilmenite crystals 1,2).

peridotites, which have equilibrated at about 1200–1300 °C at 200 km depth [15].

3. Specimen preparation and analytical techniques

Electron transparent foils of (010) oriented olivine single crystals have been prepared for TEM investigation by conventional argon ion beam milling (5 kV, 12° tilt angle). Carbon coating of the TEM-ready foil prevents charging of the specimen by the electron beam.

Transmission electron microscopy (TEM) was carried out in a Philips CM200 electron microscope operated at 200 kV with a LaB₆ electron source. The TEM used is equipped with a Gatan imaging filter GIF[®] and an EDAX X-ray analyzer. The GIF was used for acquisition of energy-filtered images applying a 20 eV window to the zero loss peak of the energy-loss spectrum. Electron energy-loss spectroscopy (EELS) was carried out using a beam diameter of 15 nm and an energy dispersion of 0.3 eV/pixel. Spectrum acquisition time was 20 s. The Fe/Ti ratio was calculated from EEL spectra that contained the Ti-L_{3,2}, the O-K and the Fe-L_{3,2} edges. The ratio calculation was done by means of the Gatan DM software package. A Hartree–Slater model was used for cross-section calculations. The background fit model applied was a power law model.

Analytical electron microscopy (AEM) was performed by means of an energy dispersive analyzer (Si–Li) with ultra-thin window. Analyses were carried out in scanning transmission mode (STEM), scanning the electron beam (beam size 4 nm) across a window the size of the inclusion. Scanning the beam over a preselected area significantly reduces beam damage during spectrum acquisition. The k_{AB} factors for quantitative analyses were determined from an olivine standard (San Carlos olivine) and an ilmenite standard; the chemical composition of the standard was measured with electron microprobe. Subsequently, a TEM foil was prepared by focused ion beam thinning (FIB) from the same sample and from precisely that volume that was measured by microprobe analysis. These foils were used as standard for AEM. Counting time was 200 s. The foil was tilted 20° towards the detector during measurements. The total relative error, which is the sum of the error (3σ at $\approx 99\%$ confidence limit) of the measured intensities plus the error in the k_{AB} factor, was calculated as: in olivine $\approx 3\%$ for SiO₂, $\approx 3\%$ for MgO, $\approx 16\%$ for FeO; in ilmenite ($\approx 3\%$ for TiO₂, $\approx 3\%$ for FeO and $\approx 10\%$ for MgO and 15% for Cr₂O₃; cf. [16]). The foil thickness necessary for absorption correction was derived from the EEL spectrum using the zero loss peak intensity (I_0) and the total spectrum (I_t) [17,18]. From total intensity of the spectrum (I_t) and the intensity of the zero loss peak (I_0) in the equation $t/\lambda = \ln(I_t/I_0)$ the ratio of specimen thickness (t) divided by the electron

mean free path (λ) is calculated. The calculated electron mean free path λ for olivine at an acceleration voltage of 200 kV is about 100 nm.

The average grain size of the inclusions is about 50 nm. Consequently, a typical foil thickness of about 100 nm will certainly include some volume of the host olivine. The following procedure was applied to subtract the X-ray intensity contribution from the host olivine to the X-ray intensities of Mg and Fe in the spectrum from the inclusion. The basic assumption is that the net intensity ratios $Mg/Si=k_1$ and $Fe/Si=k_2$ are constant for the host olivine and can be calculated. The spectrum of ilmenite contains nearly no silica as evident from the analysis of accessory ilmenite (Table 2). Consequently, if the X-ray spectrum from an inclusion contains $Si-K_{\alpha}$ intensity, additionally to $Mg-K_{\alpha}$, $Ti-K_{\alpha}$, $Cr-K_{\alpha}$ and $Fe-K_{\alpha}$ intensities, then a certain contribution of X-ray intensity from the host olivine in the spectrum must be expected. From the measured $Si-K_{\alpha}$ intensity, and the previously calculated net intensity ratio k_1 and k_2 , the X-ray intensities related to the concentration of Mg and Fe in olivine are derived. These intensities are subtracted from the total intensities of Mg and Fe measured in the spectrum, thus giving the net intensities of Mg, Ti, Cr and Fe, which are related only to the inclusion. Finally, the concentrations of MgO , TiO_2 , Cr_2O_3 and FeO are calculated using the Cliff–Lorimer equation [19]:

$$\frac{Int_{A-incl.}}{Int_{B-incl.}} = k_{A/B} * \frac{Conc_{A.}}{Conc_{B.}}$$

$$Conc_{Ti} + Conc_{Fe} + Conc_{Mg} + Conc_{Cr} = 1$$

The parameters $k_{Ti/Fe}=0.90$, $k_{Cr/Fe}=0.92$ and $k_{Mg/Fe}=0.89$ were determined by AEM from an ilmenite standard.

4. Results

Optically clear olivine single crystals (up to one mm in size) were investigated by TEM, EELS and AEM techniques. The chemical composition of the host olivine measured by electron microprobe analysis is $(Mg_{1.703}Fe_{0.283}Ti_{0.001}Mn_{0.003})_{1.990}Si_{1.002}O_4$. Under the optical microscope, the studied olivine grains show neither serpentinization nor alteration.

The microstructure on the TEM scale is characterized by low dislocation density and the absence of low angle grain boundaries (Fig. 1). This suggests that they might have been deformed, however, the deformation microstructure was annealed out in certain olivine grains during transport in the kimberlite. However, TEM bright field investigation reveals nanometre-sized idiomorphic inclusions (average grain size about 50 nm), which are homogeneously distributed in the olivine matrix on a TEM scale. The volume fraction of the inclusions is very low; it is estimated to be less than 0.001 vol.% (Fig. 1). The morphology of the inclusions is idiomorphic cube-like. The inclusions are not rods nor show lath-shaped morphology. They are much smaller than the ilmenite rods reported in olivine from Alpe Arami [1,2]. It is emphasized that not all of the investigated olivine grains from the same nodule contain such inclusions.

Two different types of inclusions are observed in the same olivine crystal. The first type of inclusion is ilmenite (determined from chemical composition and diffraction pattern). These inclusions exhibit either rectangular or some irregular shape with an average grain size in the range of 50–70 nm at lower magnification. However, at higher magnification, and especially from high-resolution images it becomes evident that this type of inclusions consists of two phases. Ilmenite is always intergrown with a narrow magnetite lamellae less than 10 nm wide (Fig. 2a). The presence of both ilmenite and magnetite are confirmed by electron diffraction data (Fig. 2b,c). The chemical

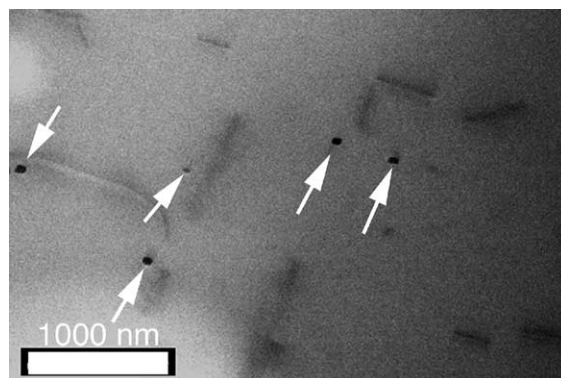


Fig. 1. TEM bright field image of nanometre-sized inclusions (arrows) of ilmenite and perovskite associated with dislocations in olivine.

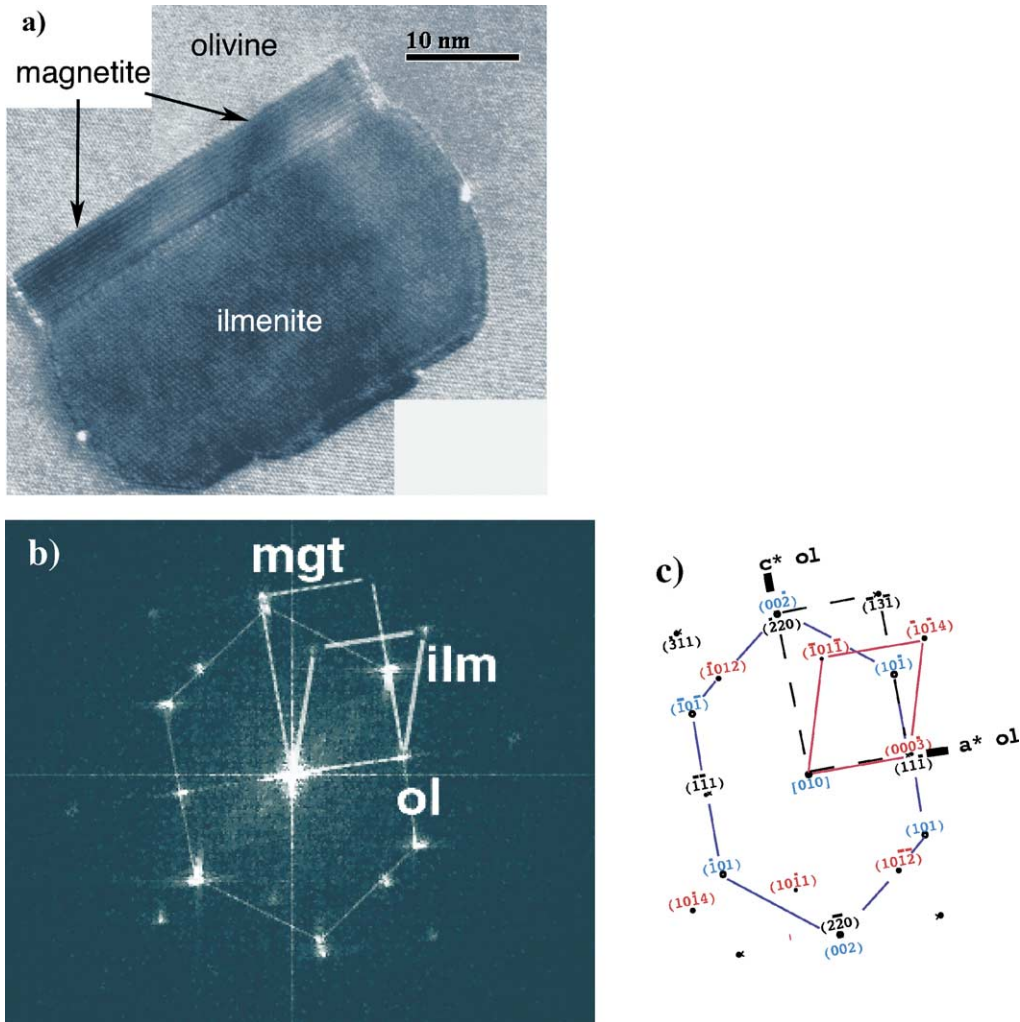


Fig. 2. Nanometre-sized inclusion of ilmenite in olivine. (a) Energy filtered TEM bright field image of a typical ilmenite inclusion intergrown with magnetite. (b) Fast Fourier Transform FFT from a high-resolution image of ilmenite+magnetite+olivine showing the orientation relationship between ilmenite–magnetite and the host olivine. (c) Simulated diffraction pattern using the experimentally derived orientation relationship of the phases involved. The simulated diffraction pattern matches the experimental diffraction pattern (b).

composition of ilmenite, determined by AEM is $(\text{Mg}_{0.34} \text{Fe}_{0.76} \text{Cr}_{0.07})_{1.17} \text{Ti}_{0.90} \text{O}_3$ (cf. Table 3). The ratio Fe/Ti is 0.84. Ilmenite inclusions are always intergrown with these narrow lamellae of magnetite. Therefore, analyses of ilmenite inclusions might contain Fe-K α intensity, which is contributed from the magnetite lamellae. This might result in an overestimate of the actual Fe-concentration in ilmenite. Line-scans across ilmenite inclusions show the presence of iron in ilmenite as well as iron and chromium in

the magnetite lamellae (Fig. 3). Occasionally, nanometre-sized magnetite lamellae are observed along more than one crystal faces of ilmenite. The orientation relationships between ilmenite, magnetite lamellae and the host olivine were determined from electron diffraction patterns and high-resolution images:

$$[010]_{\text{ol}} // [112]_{\text{mgt}} // [-12-10]_{\text{ilm}}$$

$$(100)_{\text{ol}} // (11-1)_{\text{mgt}} // (000-1)_{\text{ilm}}$$

Table 3
Chemical composition of nanometre-sized ilmenite polymorph inclusions in olivine AEM analyses

Wt.%	Ilmenite	Ilmenite (perovskite structure)
MgO	9.48	3.52
FeO	37.75	40.09
TiO ₂	49.32	49.67
Cr ₂ O ₃	3.45	6.69
Σ	100.00	99.97

Ilmenite: (Mg_{0.34} Fe_{0.76} Cr_{0.07})_{1.17}Ti_{0.90}O₃.

Perovskite: (Mg_{0.13} Fe_{0.83} Cr_{0.13})_{1.09} Ti_{0.92} O₃.

The second type of inclusion typically exhibits rectangular shape, with an average grain size of about 50 nm at low magnification (Fig. 4). Many of them have stepped interfaces with the host olivine, which is also visible by strain contrast. Characteristic features in the bright field images of the inclusions are small grooves visible as bright dots at the interface olivine/inclusion (Figs. 4 and 5). These grooves exhibit a regular spacing and can be correlated with a regular spaced diffraction contrast modulation, which is visible in certain directions. The spacing of modulated contrast pattern is about 14 nm in [201] and about 11 nm in $[\bar{1}01]$ direction (Figs. 4 and 5). Magnetite

lamellae have never been observed together with the second type of inclusion.

The chemical composition of these inclusions (Mg_{0.13} Fe_{0.83} Cr_{0.13})_{1.09} Ti_{0.92} O₃ is different from that of ilmenite inclusions (Mg_{0.34} Fe_{0.76} Cr_{0.07})_{1.17} Ti_{0.90} O₃. Mg concentration is much lower than in ilmenite, Fe and Ti are similar, whereas Cr concentration is larger than in ilmenite. Fe/Ti ratio determined from AEM measurements (whole inclusion) is 0.90, which is slightly larger than that of ilmenite. However, the Fe/Ti ratio determined by EELS (spot analyses with high spatial resolution) varies between 0.90 and 2.29. The EEL spectra were acquired with a small electron beam (spot size 15 nm) from different locations in the same sample. The small beam size allows a better spatial resolution and the varying Fe/Ti ratio is suggested to represent local inhomogeneity in the Fe and Ti concentration. Due to the short acquisition time for EEL spectra (2 s for one spectrum; 10 spectra were accumulated) beam damage can be neglected even for spot measurements. The oxygen K-edge in EEL spectra from the second type of inclusion shows a pronounced pre-edge at about 528 eV (Fig. 6). The pre-edge might be due to the presence of water [20] or due to the presence of Fe³⁺

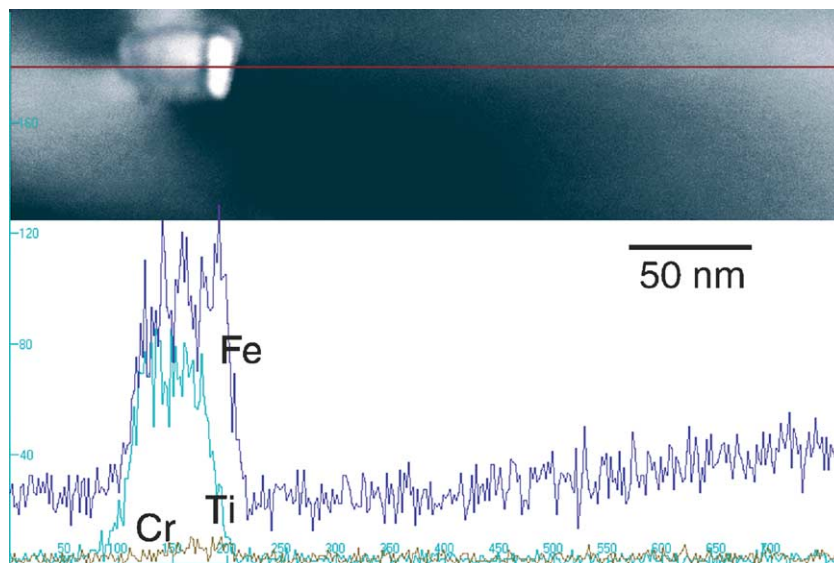


Fig. 3. Line-scan displaying the Fe-K α , Ti-K α and Cr-K α X-ray intensities across an ilmenite inclusion intergrown with a magnetite lamella. In the upper half of the figure a scanning transmission (STEM) image shows the position of the inclusions together with the trace of the scan. Note that Cr is slightly enriched in magnetite.

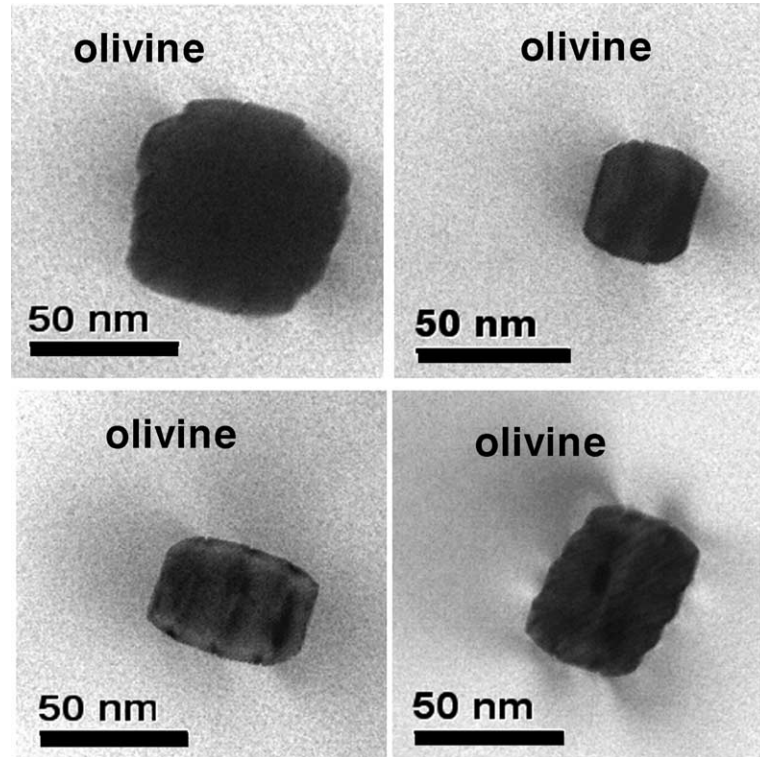


Fig. 4. Nanometre-sized perovskite inclusions in olivine. Energy filtered TEM bright field images from 4 different perovskite inclusions in olivine illustrating size and shape of the inclusions. Note the regular spaced diffraction contrast in perovskite associated with small grooves at the interface olivine/perovskite (e.g. second row, left image).

or other 3d transition metals such as titanium [21]. For ilmenite or ilmenite with perovskite structure, the presence of water can be excluded and therefore the pre-edge is assigned to the presence of Fe^{3+} and titanium. Additionally, the presence of Fe^{3+} is indicated by an asymmetric shape of the Fe-L_{3,2} edge, which consists of Fe^{2+} and Fe^{3+} contributions. From that shoulder in the Fe-L_{3,2} edge and the pronounced pre-peak prior to the onset of the oxygen K-edge it is concluded that a fraction of the total iron in perovskite is Fe^{3+} . The intensity of the pre-edge peak at about 528 eV measured in different volumes from one and the same nanocrystal varies. The diffraction pattern mentioned above might be a result of an ordering effect of trivalent iron in the perovskite structure.

Diffraction patterns of these inclusions and Fast Fourier transforms (FFT) of high-resolution images cannot be indexed using the ilmenite structure or the lithium niobate structure of the inclusions (Fig. 7a,b).

Diffraction patterns and FFT of those inclusions can be indexed only and modelled, assuming a monoclinic perovskite structure with unit cell dimensions $a_o=1.09(5)$ nm, $b_o=0.5169$ nm, $c_o=0.74(3)$ nm and a monoclinic angle $\beta=95^\circ$. The unit cell parameters a_o , c_o as well as the monoclinic angle β were derived from the experimental diffraction patterns and FFT from the HREM images (Fig. 5). Cell parameter b_o was added from literature data for FeTiO_3 with orthorhombic perovskite structure [7]. The observed crystal structure is similar to

$$(101)_{\text{olivine}} // (300)_{\text{perovskite}} \quad [010]_{\text{olivine}} // [0\bar{1}0]_{\text{perovskite}}$$

the orthorhombic cell parameters of FeTiO_3 perovskite at 18 GPa with $a_o=0.5022$ nm, $b_o=0.5169$ nm and $c_o=0.7239$ nm [7]. However, the observed a_o parameter of the inclusions is about twice the value given in literature and the orthorhombic cell is slightly monoclinic distorted. The cell parameters of ilmenite

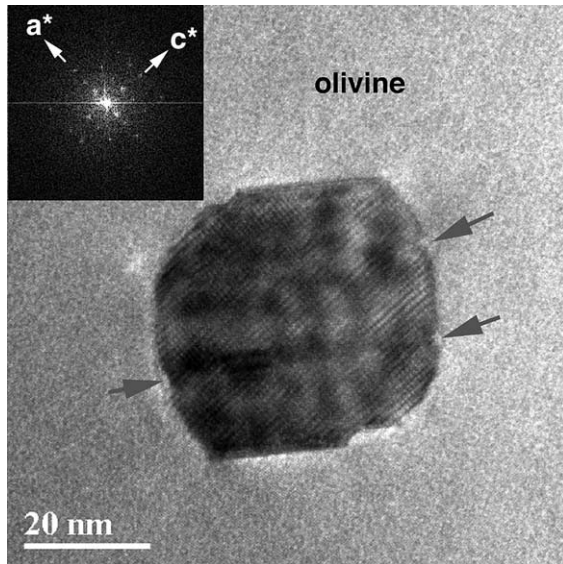


Fig. 5. Energy filtered TEM bright field image of a perovskite inclusion in olivine at higher magnification. Grey arrows indicate grooves at the interface olivine/perovskite. Modulated diffraction contrast is visible in the inclusion. The inserted corresponding diffraction pattern (FFT) with zone axis [010] exhibits the monoclinic angle $\beta=95^\circ$ of the perovskite crystal.

polymorphs such as Li-NbO₃ structure, perovskite and perovskite (this study) are given in Table 1. The differences between cell parameters from literature and observed cell parameters might be due to different

chemical composition. The experimentally observed diffraction pattern can be completely modelled based on a monoclinic distorted perovskite structure with the cell dimensions (Fig. 7b). The orientation relationship between monoclinic perovskite and the host olivine is discussed in the following section.

5. Discussion

5.1. Preservation of perovskite in olivine

Experimental studies on the stability of (Mg,Fe)-TiO₃ perovskite and ilmenite have shown that perovskite is not a quenchable phase, at least not experimentally [6–8]. The question arises, as to perovskite is preserved in the investigated olivine crystals of a nodule from a kimberlite pipe. There are several arguments, which might explain the occurrence of perovskite in our samples. In contrast to the commonly observed cracks around coesite inclusions in pyrope, which indicate a sudden pressure release, cracks are never observed around these perovskite inclusions.

Considering the volume change during the phase transformation perovskite \Rightarrow ilmenite, the volume (perovskite=50.38 Å³/formula unit) increases with the transformation to ilmenite (52.668 Å³/formula unit)

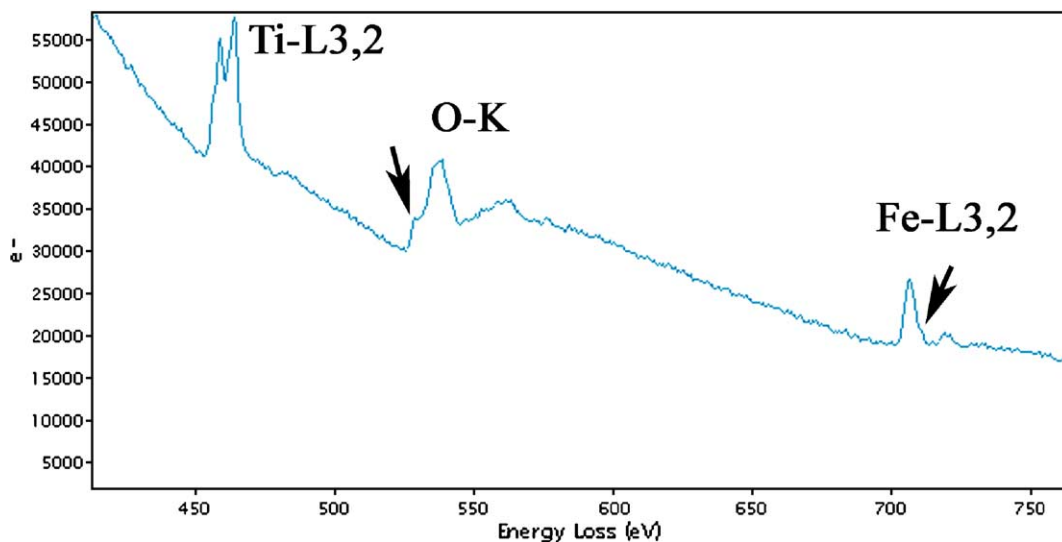


Fig. 6. EEL spectrum of perovskite including some contribution from the olivine matrix. The arrow near the O-K edge indicates the pre-edge, which in this case is indicative for the presence of Fe³⁺ titanium. The arrow at the Fe-L_{3,2} edge points to a shoulder also caused by Fe³⁺.

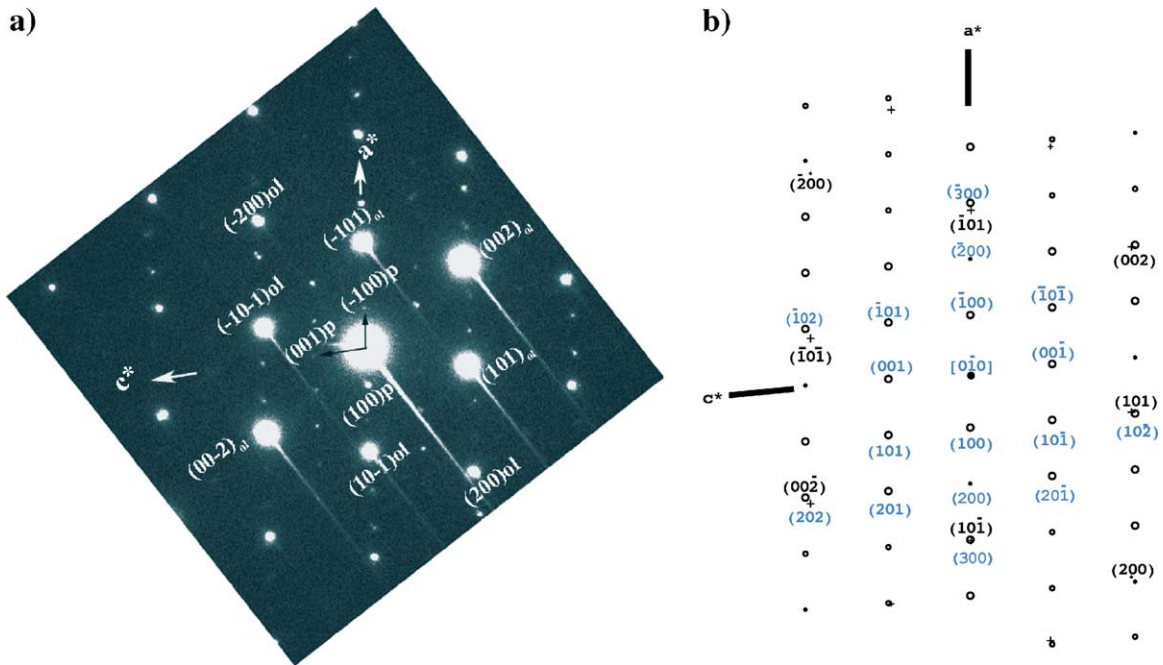


Fig. 7. Comparison of the electron diffraction pattern obtained from perovskite in olivine with the simulated diffraction pattern. (a) The electron diffraction pattern shows the reflections of olivine as spots with high intensities. Superimposed are the much weaker reflections of perovskite. $[010]$ is zone axis for both olivine and perovskite. The monoclinic angle $\beta=95^\circ$ is given by the axis a^* and c^* of perovskite. (b) Simulated electron diffraction pattern from olivine+perovskite using the experimentally determined orientation relationship between olivine and perovskite. The perovskite pattern is displayed by the symbol (O, blue indices) and the olivine pattern by crosses (+, black indices).

[7]. That volume change is about 3.3% assuming divalent Fe and tetravalent Ti in the perovskite phase, and it would be about 5% for trivalent Fe and trivalent Ti [7]. From these numbers it is concluded, that with decompression during the ascent of the nodule within the kimberlitic magma, the positive ΔV of the phase transformation perovskite \Rightarrow ilmenite stabilizes the perovskite structure. Anisotropy of thermal expansion might also support stabilization of the perovskite structure. The anisotropy of thermal expansion is $\alpha_0=9.9\times 10^{-6}$ for b_0 , $\alpha_0=9.8\times 10^{-6}$ for c_0 and $\alpha_0=6.6\times 10^{-6}$ for a_0 of olivine [22]. The thermal expansion of ilmenite is $\alpha_0=10.1\times 10^{-6}$ for a_0 and $\alpha_0=7.6\times 10^{-6}$ for c_0 [4]. The orientation relationship of the ilmenite inclusions in olivine requires that $[010]_{ilm}$ is parallel $[010]_{olivine}$. That means, the direction in olivine with the largest thermal expansion $\alpha_0=9.9\times 10^{-6}$ is parallel to the direction with largest thermal expansion in ilmenite $\alpha_0=10.1\times 10^{-6}$. Consequently, any temperature change would pose additional stress during the phase transformation on the

interface perovskite/olivine thus stabilizing the perovskite structure. One of the most striking arguments for the stability of the perovskite inclusions in olivine might be the fact that the perovskite inclusions are nanometre-sized crystals. There is evidence that phase transformations seem to be prevented by nanocrystalline morphologies [23]. For example, the phase transformation from γ -Fe to α -Fe observed in coarse-grained polycrystals does not occur in the isolated nanometre-sized crystals. Two reasons are conceivable for this effect. The small crystals do not contain suitable nucleation sites for the α -phase. Alternatively, the growth of the α -phase is inhibited [23]. Returning to the stability of the perovskite phase, we also need to consider the nucleation problem. The coherency of the interface perovskite/olivine is quite good, which is also demonstrated by the simulated diffraction pattern in Fig. 7b. However, a coherent interface will reduce the probability of nucleation of the stable ilmenite phase thus inhibiting the phase transformation.

Nevertheless, additionally to nanocrystalline perovskite inclusions we observe other nanocrystalline ilmenite inclusions in the same olivine grain. This fact requires a mechanism, which enables the transformation under certain conditions. Such a special condition can be a moving dislocation. The investigated olivine grains contain dislocations with straight or sometimes slightly curved dislocation lines (cf. Fig. 1). The curved dislocation lines indicate that the dislocations once were mobile, implying that the dislocations could have climbed by diffusion processes. Dislocations will interfere with nanocrystalline inclusions when gliding or climbing through the olivine lattice. Associated with moving dislocations is plastic deformation of the host lattice, and deformation is suggested to initiate a stress drop in the vicinity of the perovskite thus allowing perovskite to transform to ilmenite. Again, the major aspect seems to be, that we have to deal with nanocrystalline material, which shows different behaviour from that of larger crystals.

5.2. Formation of perovskite inclusions

Two different models are discussed, which can explain the observed nanocrystalline perovskite in olivine: precipitation of perovskite in olivine or overgrowth of nanometre-sized perovskite by olivine. The finding of ilmenite rods in olivine from Alpe Arami was explained by precipitation of the high-pressure perovskite polymorph of ilmenite [1]. The idea is based on the subsequently experimentally confirmed assumption that the solubility of TiO_2 in olivine exceeds 0.6 wt.% at pressures of 9–12 GPa depending on temperature [25,26]. Subsequent decompression would result in exsolution of ilmenite or TiO_2 ; however, TiO_2 is not observed in our samples. In our case, precipitation of $(\text{Mg,Fe})\text{TiO}_3$ perovskite from Ti-supersaturated olivine in the stability field of FeTiO_3 perovskite seems to be an unlikely mechanism, because not all of the olivine grains show these perovskite inclusions. It would be difficult to explain why different olivine grains from the same nodule should have incorporated different amounts of titanium. However, keeping in mind that ilmenite is also present in this nodule as a minor constituent and sometimes intergrown with garnet, it seems to be likely that the nanometre-sized perovskite crystals have formed outside olivine—possibly along

grain or phase boundaries—at a depth exceeding 300 km, and subsequently have been incorporated into olivine by moving olivine grain boundaries i.e. grain growth of olivine. Overgrowth of the nanocrystals by olivine would easily explain the absence of perovskite in some olivine grains. This interpretation is supported by the similar chemical composition of accessory ilmenite and the nanocrystalline ilmenite in olivine (c.f. Table 2).

5.3. Geological implications

What are the consequences of the presence of $(\text{Mg,Fe,Cr})\text{TiO}_3$ perovskite for the host nodule? For the investigated samples (high-temperature garnet peridotite nodules from Udachnaya-East), the temperature and pressure data given in literature are in the range of 1200–1300 °C and 6.5 GPa, which is equivalent to about 200 km [15]. Another source reports 1300–1400 °C at 3.5–4 GPa [14]. There is a remarkable difference in pressure and temperature conditions. Based on the stability curve of FeTiO_3 perovskite combined with the temperature range 1200 °C–1400 °C from literature a minimum pressure of 8 GPa at 1400 °C and 10 GPa at 1200 °C can be derived for these xenoliths (Fig. 8). An upper bound for pressure is given by the olivine $\Rightarrow\beta$ -olivine phase boundary, which limits the maximum pressure to 13–14 GPa, because we have to deal with the olivine phase. Based on a subcontinental geotherm (40 mw/m^2) [24] temperature should not have exceeded 1300 °C. However, porphyroclastic, Ti-rich peridotite xenoliths are commonly interpreted to reflect the metasomatic infiltration of a magma (the kimberlite precursor). This is assumed to represent ascending asthenospheric material and can perturb the temperatures from a normal subcontinental mantle convective geotherm. Therefore, an estimate for minimum pressure for the investigated sample at a temperature of 1300 °C would plot at about 9 GPa. In any case, the olivine grain from this particular high-temperature garnet peridotite must have experienced pressure exceeding 9 GPa (1300 °C). Assuming only 1200 °C for the host nodule the lower pressure bound would be at about 10 GPa, significantly higher than 200 km or 6.5 GPa mentioned previously [14,15]. Consequently, the nodule containing the investigated olivine must have originated from about 300 km

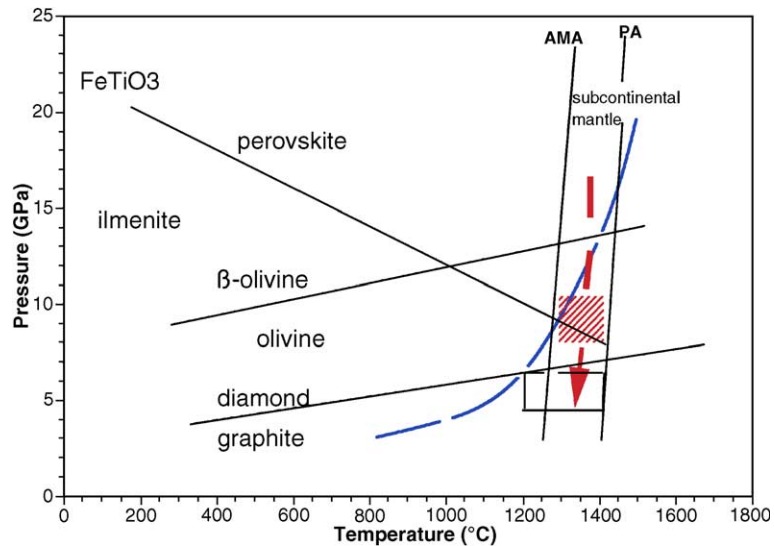


Fig. 8. Pressure–temperature diagram showing the derived region of possible P – T space for the nanometre-sized perovskite inclusions (hatched square). For the most likely equilibrium temperature interval of 1200–1300 °C of the high temperature garnet peridotites a pressure range for the host xenolith 8–10 GPa is inferred. The graphite diamond transition is from [27]; the olivine phase stability is from [12]; the ilmenite/perovskite boundary for FeTiO_3 from [8] and the subcontinental mantle geotherm (40 mW/m^2) is from [24]. The arrow indicates a possible P – T path of olivine with the inclusions. The rectangle is the range of petrologically determined P – T conditions from silicates. AMA is an average mantle adiabat and PM is an average plume adiabat (Bell, personal communication).

depth, and was equilibrated subsequently at some shallower depth between 150 and 200 km. In a recent paper on garnet inclusions containing significant majorite component in microdiamonds from kimberlitic pipes located not far from Udachnaya-East pipe (Yubileynaya and Komsomolskaya) were described. These inclusions provide an additional support for the extraction of some microdiamonds and, possibly, xenoliths from depth more than 300 km [28]. Two models for the ascent from 300 km to shallower depth can be considered. Firstly, the nodule was picked up at a depth of 300 km by the kimberlitic magma during its ascend and transported to shallower depth according to the pressure estimates from literature given above. There, it was equilibrated as inferred from thermobarometric data [14,15]. There is no information about the residence time of the nodule at shallower depth. Another kimberlitic event finally brought it to the surface. A second possibility is that the nodule was transported slowly from 300 km to shallower depth (150–200 km) by mantle convection, and finally was equilibrated at that depth before it was brought to the surface by the kimberlite eruption. If the second mechanism would apply, then it would be hard to

understand how the nanometre-sized perovskite could have survived and not reacted with olivine.

6. Summary

Contradicting experimental results on the stability and quenchability of $(\text{Mg,Fe,Cr})\text{TiO}_3$ perovskite, under special conditions, perovskite can be preserved as inclusions in olivine, thus providing a geobarometer for xenoliths originating deep within kimberlite sources. The most important condition for the perovskite structure to survive is that perovskite occurs as nanometre-sized inclusions. The nanometre size of the perovskite inclusions together with a positive ΔV during the phase transition perovskite \rightarrow ilmenite, and the anisotropic thermal expansion prevents the phase transformation, which occurred with perovskite in the matrix. All of the accessory ilmenite might have been previously perovskite. The presence of perovskite in olivine from an ilmenite–garnet–peridotite nodule from the kimberlite pipe Udachnaya, Siberia allows a new pressure estimate for that nodule. Deviating from literature data, which

give a maximum depth of 200 km for such kind of nodule, our new pressure estimate, based on the perovskite stability, is about 300 km.

Acknowledgements

Many fruitful discussions with L. Dobrzhinetskaya strongly encouraged writing this paper. Suggestions from F. Schilling concerning mineral physics problems with small inclusions in a host mineral are gratefully acknowledged. D. Lattard is thanked for valuable discussions. The authors would like to thank K. Peach for skilful TEM sample preparation. W. Heinrich is thanked for comments and suggestions and for critically reading the manuscript. The constructive reviews of the paper by D. Bell and N. Sobolev are gratefully acknowledged. Comments of D. Bell concerning Fig. 8 and the geological implications substantially improved that figure.

References

- [1] L. Dobrzhinetskaya, H.W. Green II, S. Wang, Alpe Arami: a peridotite massif from depths of more than 300 kilometres, *Science* 271 (1996) 1841–1845.
- [2] K.N. Bozhilov, H.W. Green II, L.F. Dobrzhinetskaya, Quantitative 3D measurement of ilmenite abundance in Alpe Arami olivine by confocal microscopy: confirmation of high-pressure origin, *Am. Mineral.* 88 (2003) 596–603.
- [3] A.-C. Risold, V. Trommsdorff, B. Grobety, Genesis of ilmenite rods and palisades along humite-type defects in olivine from Alpe Arami, *Contrib. Mineral. Petrol.* 140 (2001) 619–628.
- [4] B.A. Wechsler, C.T. Prewitt, Crystal structure of ilmenite (FeTiO₃) at high temperature and at high pressure, *Am. Mineral.* 69 (1984) 176–185.
- [5] Y. Syono, H. Yamauchi, A. Ito, Y. Someya, E. Ito, Y. Matsui, M. Akaogi, S. Akimoto, Magnetic properties of the disordered ilmenite FeTiO₃ II synthesized at very high pressure, *Ferrites: Proceedings of the International Conference, Japan, 1980*.
- [6] K. Leinenweber, J. Linton, A. Navrotsky, Y. Fei, J.B. Parise, High-pressure perovskites on the join CaTiO₃–FeTiO₃, *Phys. Chem. Miner.* 22 (1995) 251–258.
- [7] K. Leinenweber, W. Utsumi, Y. Tsuchida, T. Yagi, K. Kurita, Unquenchable high-pressure perovskite polymorphs of MnSnO₃ and FeTiO₃, *Phys. Chem. Miner.* 18 (1991) 244–250.
- [8] A. Metha, K. Leinenweber, A. Navrotsky, M. Akaogi, Calorimetric study of high-pressure polymorphism in FeTiO₃: stability of the perovskite phase, *Phys. Chem. Miner.* 21 (1994) 207–212.
- [9] E. Ito, Y. Matsui, High-pressure transformations in silicates, germinates, and titanates with ABO₃ stoichiometry, *Phys. Chem. Miner.* 4 (1979) 265–274.
- [10] J.A. Linton, Y. Fei, A. Navrotsky, Complete Fe–Mg solid solution in lithium niobate and perovskite structures in titanates at high pressures and temperatures, *Am. Mineral.* 82 (1997) 639–642.
- [11] S.P. Clark, A.E. Ringwood, Density distribution and constitution of the mantle, *Rev. Geophys.* 2 (1964) 35–42.
- [12] M. Akaogi, E. Ito, A. Navrotsky, Olivine-modified spinel–spinel transitions in the system Mg₂SiO₄–Fe₂SiO₄: calorimetric measurements, thermochemical calculation, and geophysical application, *J. Geophys. Res.* 94 (1989) 15671–15685.
- [13] V.S. Sobolev, N.L. Dobretsov, N.V. Sobolev, Classification of deep seated xenoliths and the type of the upper mantle, *Geol. Geophys. N12* (1972) 37–42 (in Russian).
- [14] E.E. Lazzko, *Minerali-sputniki Almaza I Genesis Kimberlitovich Porod, Nedra, Moscow, 1979*, 192 pp. (in Russian).
- [15] F.R. Boyd, N.P. Pokhilenko, D.G. Pearson, S.A. Mertzman, N.V. Sobolev, L.W. Finger, Composition of the Siberian cratonic mantle: evidence from Udachnaya peridotite xenoliths, *Contrib. Mineral. Petrol.* 128 (1997) 228–246.
- [16] M. Koch-Müller, R. Wirth, An experimental study of the effect of iron on magnesiochloritoid–talc–chloritoid–kyanite stability, *Contrib. Mineral. Petrol.* 141 (2001) 546–559.
- [17] T. Malis, S.C. Cheng, R.F. Egerton, EELS log-ratio technique for specimen thickness measurement in the TEM, *J. Electron Microsc. Tech.* 8 (1988) 193–200.
- [18] R.F. Egerton, *Electron Energy-loss Spectroscopy in the Electron Microscope*, Plenum Press, New York.
- [19] G. Cliff, G.W. Lorimer, The quantitative analysis of thin specimens, *J. Microsc.* 103 (1975) 203–207.
- [20] R. Wirth, Water in minerals detectable by electron energy-loss spectroscopy EELS, *Phys. Chem. Miner.* 24 (1997) 561–568.
- [21] P.A. van Aken, B. Liebscher, V.J. Styrsa, Core level electron energy-loss spectra of minerals: pre-edge fine structures at the oxygen K-edge, *Phys. Chem. Miner.* 25 (1998) 561–568.
- [22] I. Suzuki, Thermal expansion of periclase and olivine and their anharmonic properties, *J. Phys. Earth* 23 (1975) 145–159.
- [23] H. Gleiter, Nanocrystalline materials, *Prog. Mater. Sci.* 33 (1989) 223–315.
- [24] H.N. Pollack, D.S. Chapman, On the regional variation of heat flow, geotherms and lithosphere thickness, *Tectonophysics* 38 (1977) 279–296.
- [25] L. Dobrzhinetskaya, K.N. Bozhilov, H.W. Green II, The solubility of TiO₂ in olivine: implications for the mantle wedge environment, *Chem. Geol.* 163 (2000) 325–338.
- [26] D. Tinker, C.E. Leshner, Solubility of TiO₂ in olivine from 1 to 8 GP, *EOS Transactions of the American Geophysical Union* 82, Fall Meet. Supplement, Abs#V51b-1001.
- [27] C.S. Kennedy, G.C. Kennedy, The equilibrium boundary between graphite and diamond, *J. Geophys. Res.* 81 (1976) 2467–2470.
- [28] N.V. Sobolev, A.M. Logvinova, D.A. Zedgenizov, E.S. Yefimova, Y.V. Seryotkin, K. Floss, L.A. Taylor, Mineral inclusions in microdiamonds and macrodiamonds from Yakutian kimberlites: a comparative study, *Lithos* 77 (2004) 225–242.